Metabolic modeling for predicting VFA production from protein-rich substrates by mixed-culture fermentation

Alberte Regueira, Juan M. Lema, Marta Carballa, Miguel Mauricio-Iglesias

Supporting Information

Supporting Information

Metabolic modelling for predicting VFA production from protein-rich substrates

A. Regueira*, J. M. Lema, M. Carballa, M. Mauricio-Iglesias.

Department of Chemical Engineering, Institute of Technology, Universidade de Santiago de Compostela, 15782 Santiago de Compostela, Spain

*Corresponding author (e-mail: alberte.regueira@usc.es)

1. MODEL DESCRIPTION

A. Mass balances

The mass balances for each of the compartments are defined by the following equations (Eq. S1-S4).

Intracellular compounds

$$\frac{dS_i}{dt} = R_i + R_{T,i} \quad \text{(S1)}$$

Where S_i is the intracellular concentration (mol L_x^{-1}), R_i and $R_{T,i}$ are, respectively, the reaction rate and intra-extra cellular transport rate (mol L_x^{-1} h^{-1}).

Extracellular compounds

$$\frac{dS_k}{dt} = D_{liq} \cdot \left(S_{K,in} - S_k\right) + R_{T,k} \quad \text{(S2)}$$

Where S_k is the extracellular concentration (mol L_{liq}^{-1}), D_{liq} is the liquid dilution rate (h^{-1}), $S_{K,in}$ is the concentration on the inlet (mol L^{-1}) and $R_{T,j}$ is the intra-extra cellular transport rate (mol L_{liq}^{-1} h^{-1}).

Biomass

$$\frac{dS_X}{dt} = -D_{liq} \cdot S_X + R_{ana} - R_{decay} \quad \text{(S3)}$$

Where S_X is the biomass concentration (mol L_r^{-1}), R_{ana} is the anabolism rate and R_{decay} the decay rate.

Gas compounds

$$\frac{dG_m}{dt} = -D_{gas} \cdot G_m + R_{T,m} \quad \text{(S4)}$$

Where G_m is the concentration (mol L_{gas}^{-1}), D_{gas} is the gas space dilution rate (h^{-1}) and $R_{T,m}$ is liquid-gas transport rate (mol L_{gas}^{-1} h^{-1}).

More detailed information on how the different reaction and transport rates are determined can be found in sections B to G.

B. Acid-base speciation

The states of the model are the concentration of the different metabolites that participate in the cell metabolism. They account for all the possible forms of a compound that depend on acid-base equilibria (i.e. with different degrees of protonation). However, to accurately describe some processes, the concentration of a certain form of a compound is needed (e.g. the concentration of the electrically neutral form is needed to describe passive transport). The calculation of the different forms of each compound is done following the procedure described in González-Cabaleiro *et al.* (González-Cabaleiro, Lema, & Rodríguez, 2015).

C. Thermodynamic feasibility

In some cases, some degradation pathways might be endergonic. The thermodynamic feasibility of the pathways should be addressed to let the model prevent certain pathways depending on their change of Gibbs free energy (ΔG). For each of the degradation pathways and at each time step their ΔG is calculated and their feasibility factor (*f*) is determined. This factor is a step function that varies between 0, when the reaction is endergonic and should not happen, and 1, when the reaction is sufficiently exergonic and can run without limitations. A minimum feasible value for ΔG of -2 kJ/mol is assumed to consider a reaction to run. The threshold value and determination of the ΔG values are done following González-Cabaleiro et al. (2015)*(González-Cabaleiro et al., 2015; González-Cabaleiro, Lema, Rodríguez, & Kleerebezem, 2013)*.

All step function used in the model are expressed as derivable functions and follow the next general form:

$$f(x) = a \cdot \tanh(x + b) + c \tag{S5}$$

Where *a*, *b* and *c* are constants to modify the shape and limits of the resultant curve and *x* is the function input.

Given that this factor varies continuously between zero and one, there are values of ΔG close to -2 kJ/mol that result in intermediate values, meaning that the reaction does run but

at a lower rate. This is in accordance with LaRowe *et al.* (LaRowe, Dale, Amend, & Van Cappellen, 2012).

D. Kinetics

As stated in the hypotheses of the model (section 2.2 in the main text), we do not expect that kinetic differences among the degradation pathways of the different substrates affect the predicted product spectrum. All catabolic reactions arising from an amino acid (AA) are assumed to have the same rate as the consumption rate of that AA. The uptake rate of each individual AA is modelled with a Monod-like equation (Eq. S6) with a common maximum uptake rate for all AA of 0.75 mol AA/mol_X·h and a common affinity constant for all AA of 1 mM, meaning that there are 17 independent AA uptake rates. The values are equal to the rate values used in González-Cabaleiro et al. (2015) for glucose.

$$r_{S,AA_i} = {r_{S,AA}}^{max} \cdot \frac{S_{AA_i}}{K_S + S_{AA_i}} \quad \left(\frac{mol\ AA_i}{mol\ X \cdot h}\right) \tag{S6}$$

Where $r_{S,AAi}$ is the uptake rate of the ith AA, $r_{S,AAmax}$ is the maximum uptake ratio, S_{AAi} is the total bulk concentration of the ith AA and K_S is the AA affinity constant.

Subsequent reactions within the degradation pathways of the AA are modelled to have the same rate as the consumption rate of the AA they originated (Eq. S7).

$$R_i = f_i \cdot \nu_i \cdot r_{S,AA} \cdot z_i \cdot S_x \cdot \frac{V_R}{V_X} \quad \left(\frac{mol\ i}{L_x \cdot h}\right) \tag{S7}$$

Where, for the ith reaction, R_i is the reaction rate, fi is the feasibility factor of the reaction, ν_i is the stoichiometry factor between the reaction and the AA uptake, z_i is the reaction selection parameter (see section 2.3 in the main text), S_X is the biomass concentration, V_R is the reactor volume and V_X is the biomass volume in the reactor.

E. Anabolism and Decay

Biomass formation is only considered from AA as proteins are the only carbon and nitrogen source in this model. Biomass is assumed to be formed from an equimolar mixture of the 17 different AA because we could not find any specific information about AA proportions in typical biomass. We use a lumped stoichiometry (Eq. S8) with a certain degree of decarboxylation (González-Cabaleiro et al., 2015; Tobajas & Garcia-Calvo, 1999). The degree of decarboxylation varies with the substrate and is assumed to be dependent on the

heat of combustion of the substrate (Gommers, Vanschie, Vandijken, & Kuenen, 1988), which in turn can be easily correlated with the degree of reduction (Gary, Frossard, & Chenevard, 1995). To make a general lumped reaction that could be used for different proteins as anabolic substrate, a mean degree of reduction value of 4 was chosen, which leads to a carboxylation degree of 15% (in terms of moles of carbon of the substrate). The ATP needed to form biomass is set to 2 mol ATP/C-mol biomass, as in anabolism from glucose, because specific information for biomass growth on protein could not be found (González-Cabaleiro et al., 2015; Tobajas & Garcia-Calvo, 1999).

$$\sum_{i=AA}\left(\frac{1}{17}\cdot AA_i\right) + 9.34\ H_2O + 7.80\ ADP + 7.80\ P_i = 3.90\ X + 0.69\ CO_2 + 0.69\ NH_4^+ + 10.01\ H^+ \quad \text{(S8)}$$

For decay we consider the same equation but in the forward direction and also glucose-forming decay as modelled in González-Cabaleiro et al. (2015), since polysaccharides are as well one of the main constituents of biomass (Stouthamer, 1973). Both decay reactions are modelled to have the same rate value (Eq. S11).

The participation of electron carriers in anabolism is neglected to simplify the modelling procedure but we do not expect that their non-consideration compromises the results of the model (González-Cabaleiro et al., 2015).

Anabolism and decay rates are modelled to depend on energy availability, determined by the Gibbs energy of ATP formation. A value higher than 50 kJ/mol ATP indicates that cells have enough energy to grow. If the value is lower than 50 kJ/mol ATP, decay processes take place to regain energy. Anabolism rate is described with a Monod-like equation (Eq. S10), in which the maximum rate term is variable and dependent on energy availability (Eq. S9).

$$k_{ana} = \frac{\Delta G_{ATP} - 50}{5} \quad \left(\frac{mol\ X}{mol\ X \cdot h}\right) \quad \text{(S9)}$$

Where k_{ana} is the anabolism maximum rate and ΔG_{ATP} is the Gibbs energy of ATP formation.

$$R_{ana} = k_{ana} \cdot \frac{\sum_{i=AA} S_{k,i}}{M_{ana} + \sum_{i=AA} S_{k,i}} \cdot S_X \quad \left(\frac{mol\ X}{L_r \cdot h}\right) \quad \text{(S10)}$$

Where R_{ana} is the anabolism rate, $S_{k,i}$ is the extracellular concentration of the ith AA in carbon molar basis and M_{ana} is the anabolism affinity constant (1e-6 C-mol/L).

Decay rate is only controlled by the Gibbs energy of ATP formation (Eq. S11)

$$R_{decay} = \frac{50 - \Delta G_{ATP}}{5} \cdot S_X \quad \left(\frac{mol\ X}{L_r \cdot h}\right) \tag{S11}$$

F. Transport

Cells have evolved semi-permeable membranes that allow for both uncontrolled passive transport and controlled active transport. Uncharged molecules diffuse freely through the membrane, as for example the protonated form of VFA. Charged molecules and big neutral molecules (glucose or non-charged AA) cannot diffuse across the membrane and must be transported actively by a wide set of channel proteins that are controlled by the cell (David White, Drummond, & Fuqua, 2012).

Passive transport (Eq. S12) is energetically uncoupled to microorganisms and is governed by Fick's Law (i.e. transport follows the concentration gradient of each compound). There is little data available in literature about diffusion coefficients (k_{Diff}) for the different species modelled but values used in previous modelling works are in the same order of magnitude (González-Cabaleiro et al., 2015; Rodriguez, Kleerebezem, Lema, & van Loosdrecht, 2006; Zhang, Zhang, Chen, van Loosdrecht, & Zeng, 2013). Following González-Cabaleiro et al. (2015) approach we choose to give the same value to all the diffusion coefficients (100 $L/mol_X\ h$), as the main divergencies among the transport rates will be caused by the differences in their acidification degree (i.e. proportion between the charged and uncharged form of a molecule following acid-base equilibrium), which are already accounted for in the model (section B).

$$R_{Diff,i} = k_{Diff} \cdot \left({S_{k,i}}^{uncharged} - {S_{i,i}}^{uncharged}\right) \cdot X \cdot \frac{V_R}{V_X} \left(\frac{mol\ i}{L_x \cdot h}\right) \tag{S12}$$

Where, for the ith compound, $R_{Diff,i}$ is the passive transport rate, k_{Diff} is the diffusion coefficient, ${S_{k,i}}^{uncharged}$ is the extracellular uncharged concentration and ${S_{i,i}}^{uncharged}$ is the intracellular uncharged concentration.

Active transport, on the contrary, is coupled energetically to microorganisms and can be performed against or in favour of the electrochemical gradient and spend or gain energy, respectively. These channel proteins (or ports) are modelled to be coupled to proton translocations. Negatively charged molecules (e.g. anions of organic acids) are transported with a symporter with protons and positively charged molecules (e.g. ammonium) are transported in antiport with protons, to make the process transport electrically neutral.

As an enzymatically controlled process, active transport is also modelled with a Monod-like equation (Eq. S13). We assumed that the maximum active transport ratio is equal to the maximum production rate of that compound being transported (Eq. S14). Eq. S15 determines the active transport rate.

$$r_{Act,i} = {r_{Act,i}}^{max} \cdot \frac{S_i}{K_T + S_i} \qquad \left(\frac{mol\ i}{mol\ X \cdot h}\right) \tag{S13}$$

Where, for the ith compound, $r_{Act,i}$ is the active transport rate, ${r_{Act,i}}^{max}$ is the maximum active transport rate, S_i is the intracellular concentration and K_T is the active transport affinity constant (0.15 M).

$${r_{Act,i}}^{max} = \sum_{j=AA} \nu_{i,j} \cdot {r_{S,AA}}^{max} \quad \left(\frac{mol\ i}{mol\ X \cdot h}\right) \tag{S14}$$

Where $\nu_{i,j}$ is the stoichiometric coefficient of compound i in the degradation reaction of AA j.

$$R_{Act,i} = r_{Act,i} \cdot X \cdot \frac{V_R}{V_X} \qquad \left(\frac{mol\ i}{L_x \cdot h}\right) \tag{S15}$$

Intracellular metabolic concentrations above 10 mM are considered not physiologically compatible (González-Cabaleiro et al., 2013) and rarely measured above this value (Bar-Even, Flamholz, Noor, & Milo, 2012). When the concentration of one actively transported compound reaches this value, active transport rate is calculated with Eq. S16, preventing thus a higher accumulation.

$$R_{Act,i} = R_i - R_{Diff,i} \quad \left(\frac{mol\ i}{L_x \cdot h}\right) \tag{S16}$$

Finally, total transport is the sum of both transport mechanisms (Eq. S17).

$$R_{T,i} = R_{Diff,i} + R_{Act,i} \qquad \left(\frac{mol\ i}{L_x \cdot h}\right) \tag{S17}$$

Where $R_{T,i}$ is the total transport rate.

If the transport of a certain compound is exergonic energy can be conserved by translocating a proton to the cytoplasm. Likewise, if a transport reaction is endergonic it can be fuelled by ATP (through a proton translocation coupled to ATP hydrolysis).

AA molecules are modelled to be transported inwards by active transport because they are either electrically charged and/or are not small enough to freely diffuse across cell membranes. However, it is not clear how their transport is coupled to the energetics of microorganisms. Studies are more focused on describing the characteristic of the ports and how they are controlled than on how transport is coupled with the energetic part of metabolism (Berger, 1973; Guidotti, Borghetti, & Gazzola, 1978; Heyne, de Vrij, Crielaard, & Konings, 1991; Meister, 2016; Oxender & Christensen, 1963; Poole, 1978). Some AA transport mechanisms appear to be stoichiometrically linked to Na^+ or proton intrusion but it is not clear whether they use the energy of those movements or not (Poole, 1978). AA intake mechanisms are therefore left uncoupled to cell energetics in the model due to lack of information.

Abiotic transport of H_2 and CO_2 between the liquid phase and the gas head space is modelled following Henry's Law and as described in González-Cabaleiro et al. (2015).

G. Energetics evaluation

The model considers that cell energetics revolves around ATP: the energy gained in catabolism or transport is stored in form of phosphate bonds in ATP and all energetic needs are satisfied by hydrolysing those phosphate bonds to generate ADP, Pi and useable energy. This energy can then be invested in growth, maintenance or fuelling active transport against the electrochemical gradient. The balance of ATP in catabolism is composed of five terms, which are described down below.

Substrate-level phosphorylation (SLP)

ATP can be directly generated by catabolic reactions. The contribution of SLP to the global ATP balance can hence be calculated straightforwardly from the reaction rates and the stoichiometry (Eq. S18)

$$R_{ATP,SLP} = \sum_i R_i \cdot \nu_{ATP,i} \quad \text{(S18)}$$

Where $R_{ATP,SLP}$ is the production rate of ATP by SLP.

Proton translocation

The cell membrane acts like a capacitor. In some exergonic metabolic steps, microorganisms can extrude a proton from the cytoplasm to the medium, storing thus energy in the membrane as its electric potential difference rises. When that proton re-enters the cell, it does it through a channel protein (ATPase) and lowers the membrane potential as a result. The energy released is stored in ATP molecules, following the chemiosmotic theory (González-Cabaleiro et al., 2013). Conversely, an ATP molecule can be broken to release energy and extrude protons that will fuel endergonic processes when re-entering the cell.

The energy needed to extrude a single proton and the number of protons needed to yield an ATP molecule depends on the proton motive force (pmf, i.e. the electrochemical potential energy of a proton). The energy needed for translocating a proton is calculated using Eq. S19.

$$\Delta\mu_{H^+} = F \cdot \Delta\psi + R \cdot T \cdot ln\left(\frac{{H^+}_k}{{H^+}_i}\right) \qquad \left(\frac{kJ}{mol\ H^+}\right) \quad \text{(S19)}$$

Where $\Delta\mu_{H+}$ is the pmf, F is the Faraday constant, $\Delta\psi$ is the difference between the extracellular and intracellular electric potential, R is the gas constant, T the temperature, ${H^+}_k$ is the extracellular proton concentration and ${H^+}_i$ the intracellular proton concentration.

The electric potential of the membrane is considered to be 0 V on the outside and -0.2 V on the inside. The electric potential is considered to be constant, meaning that processes increasing membrane electrical potential are balanced with processes decreasing it. Intracellular pH is also considered constant at a value of 7, leaving extracellular pH as the only variation source for the pmf. In those reactions where we consider the possibility of a proton extrusion, it is evaluated in each simulation step whether the energy available is high enough for extruding a proton (i.e. if it is higher that the pmf). In case the reaction is not exergonic enough, the same reaction without a proton extrusion is considered. The energy released by proton intrusion is converted into ATP. The rate at which ATP is produced by proton translocations is calculated with Eq. S20.

$$R_{ATP,pmf} = R_{H^+,pmf} \cdot \frac{\Delta\mu_{H^+}}{\Delta G_{ATP}} \quad \text{(S20)}$$

Where $R_{ATP,pmf}$ is the ATP formation rate due to proton translocations and $R_{H+,pmf}$ is the proton rate across the membrane due to proton translocations.

Transport

Active transport of end products is modelled to occur concomitantly with proton transport inwards or outwards, depending on the electric charge of the product being transported. Logically, protons being transported across the membrane exchange energy with the cell and accordingly it should be accounted for. Moreover, the transport of an end product can be against or in favour of its concentration gradient, consuming or releasing energy, respectively. This energy exchange is coupled to proton extrusion as well, resulting in a net production or consumption of ATP (Eq. S21).

$$R_{ATP,Transport} = \left(\frac{R \cdot T \cdot ln\left(\frac{S_i}{S_k}\right) - z_i \cdot F \cdot \Delta\psi}{\Delta\mu_{H^+}} + z_i \right) \cdot \frac{\Delta\mu_{H^+}}{\Delta G_{ATP}} \cdot R_{Act,i} \qquad \text{(S21)}$$

Where $R_{ATP,Transport}$ is the ATP formation rate associated to active transport

Maintenance

Energy requirements for cell maintenance are considered to be directly correlated with the biomass concentration (4.5 kJ/mol_{Cx} h). Therefore, the ATP consumption is calculated with Eq. S22.

$$R_{ATP,maintenance} = -\frac{4.5}{\Delta G_{ATP}} \qquad \text{(S22)}$$

Where $R_{ATP,maintenance}$ is the ATP consumption rate due to maintenance

Homeostasis

Intracellular pH is maintained around a value of 7 with a Na^+/H^+ antiporter (Padan, Zilberstein, & Schuldiner, 1981). It is modelled like a proportional controller with a setpoint of an intracellular pH of 7. Extracellular Na^+ concentration is set equal to its intracellular concentration at each simulation step as we consider that microorganisms would choose the cation (e.g. Na^+ or K^+) that requires less energy to be transported (i.e. that has the minimum concentration gradient). To calculate its ATP cost the equation for active transport (Eq. S21) is used considering that the intra and extracellular Na^+ concentrations are equal, resulting in Eq. S23.

$$R_{ATP,homeostasis} = \frac{R \cdot T \cdot ln\left(\frac{{H^+}_k}{{H^+}_i}\right)}{\Delta\mu_{H^+}} \cdot R_{Na^+/H^+} \quad \text{(S23)}$$

Where $R_{ATP,homeostasis}$ is the ATP spent in homeostasis.

2. METABOLIC NETWORK CONSTRUCTION

H. Electron carriers

Reduction and oxidation reactions happening in the metabolic network involve different electron carriers (EC). In the proposed network we consider two of them: ferredoxin (Fd_{red}/Fd_{ox}) and NADH ($NADH/NAD^+$). Fd_{red}/Fd_{ox} is characterized by its low redox potential ($E^{0'} \approx -400$ mV and $E' \approx -500$ mV (Wolfgang Buckel & Thauer, 2013)) and because it is the only EC capable of reducing protons to H_2. It is considered that is related with high exergonic reactions (e.g. decarboxylations) and that all the Fd_{red} yielded eventually produces H_2 by cytoplasmic ferredoxin:proton reductases (Ech) or formate when reduces CO_2 by ferredoxin:CO_2 oxidoreductases. The production of H_2 and CO_2 versus formate is in a thermodynamic equilibrium ruled only by the pH (González-Cabaleiro et al., 2015; Hoelzle, Virdis, & Batstone, 2014; Temudo, Kleerebezem, & van Loosdrecht, 2007). The couple $NADH/NAD^+$ has a higher redox potential than Fd_{red}/Fd_{ox} ($E^{0'} = -320$ mV(David White et al., 2012), $E' = -280$ mV (Wolfgang Buckel & Thauer, 2013)) and it is involved in most of the redox reactions occurring in the metabolic network (González-Cabaleiro et al., 2015; Kleerebezem, Rodriguez, Temudo, & van Loosdrecht, 2008).

I. Energy conservation

We assume that microorganisms conserve energy in two ways. Through substrate level phosphorylation (SLP) microorganisms can yield ATP, transferring a phosphoryl group ($PO3^-$) from a metabolite to ADP. Alternatively, microorganisms can extrude one proton outside the cells against its electrochemical gradient (pmf), when coupled to sufficiently exergonic reactions. That same proton will be used to produce ATP when returning to the cytoplasm. Nevertheless, extruding a proton requires a complex enzymatic machinery, meaning that there is not a proton extrusion in all the steps that energetics would theoretically allow for it. In our network we only allocated a proton extrusion wherever we found experimental literature evidence about it.

Usually, to introduce a phosphoryl group in an organic molecule, it has to be previously activated with the cofactor coenzyme-A (CoA-SH), forming a thioester. Then the CoA cofactor is swapped by a phosphoryl group and is eventually transferred to an ADP molecule to give ATP (the SLP process). However, the activation reaction is endergonic (+30-50 kJ/mol) and therefore must be linked to exergonic reactions, as for example decarboxylations. When there is no exergonic reaction to link the CoA activation, the CoA

group is transferred directly from other metabolite containing it. In this case the donor molecule loses the possibility of conserving energy by SLP. This consideration is important when constructing the network as the number of ATP molecules yielded in each pathway has a big impact in the model solution.

J. Amino acids yielding other amino acids

Some AA are interconverted to others instead of being degraded to volatile fatty acids (VFA). This is the case, for example, of glutamine and asparagine, that are the amides of glutamate and aspartate, respectively. In this case we considered that the common AA acts like a node, and the degradation pathways of these AA end in another AA and not in the final products (i.e. VFA).

K. Degradation of pyruvate and acetyl-CoA

Pyruvate and acetyl-CoA are catabolic nodes in all forms of life. They are also present most of the pathways leading to the production of VFA. To simplify the network description in the main text, the common pathway of pyruvate and acetyl-CoA degradation is described here in each of the AA that have pyruvate or acetyl-CoA as a metabolite.

Pyruvate acts as a central node (Fig. S1) in the production of the VFA of 2 to 4 carbons and ethanol. It can either be the starting point of the propionate pathway or be dehydrogenised and decarboxylated to acetyl-CoA. In this step, together with acetyl-CoA, reduced ferredoxin is produced. Acetyl-CoA can be the precursor for acetate, ethanol and butyrate. Ethanol is not accompanied by energy conservation but in both acetate and butyrate pathways there is an ATP yielding step.

Crotonyl-CoA is an intermediate in the butyrate yielding pathway. The crotonyl-CoA reduction with NADH to butyryl-CoA in the butyrate pathway is a very exergonic step ($\Delta G'^{m}$=-57 kJ/mol), indicating that it is probable that energy is conserved in this step. Literature indeed reports energy conservation via proton translocation (Wolfgang Buckel & Thauer, 2013; González-Cabaleiro et al., 2015; Li et al., 2008) but also indicates that another biochemical mechanism might take place: electron bifurcation (EB). EB is a mechanism by which cells can couple endergonic reactions with sufficiently exergonic ones (Wolfgang Buckel & Thauer, 2018; Peters, Miller, Jones, King, & Adams, 2016). It was experimentally detected that in this step the exergonic crotonyl-CoA reduction is coupled to the endergonic reduction of Fd_{ox} by NADH, which eventually will yield H_2 (Li et al., 2008). In a previous contribution, it was seen that EB reduces the discrepancies between the predicted and

experimental results (Regueira, González-Cabaleiro, Ofiţeru, Rodríguez, & Lema, 2018). Both possibilities are included in all the crotonyl-CoA reductions featured in the metabolic network.

Fumarate reduction to succinate is a similar metabolic step to crotonyl-CoA reduction in terms of energetics and reaction mechanisms (a hydrogenation of a double carbon bond). However, only energy conservation via proton translocation is reported in literature and therefore EB is not placed as an option in this step (W. Buckel, 2001; Herrmann, Jayamani, Mai, & Buckel, 2008).

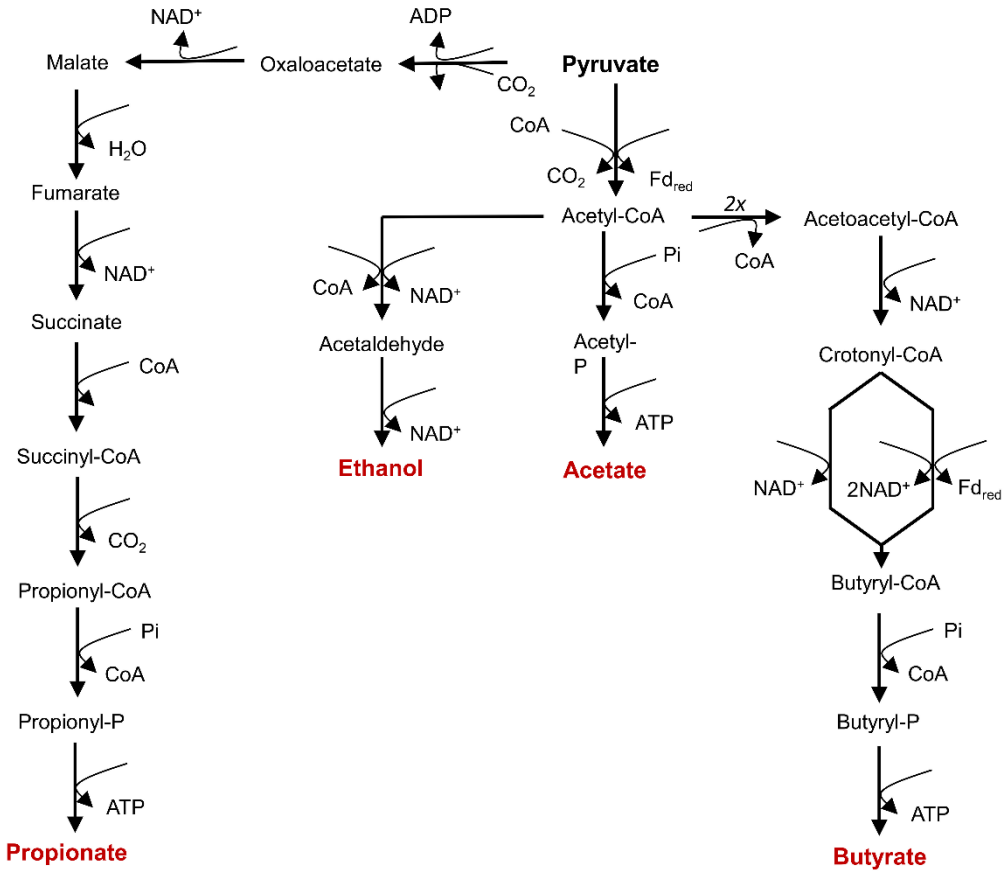

Fig. S1 Pyruvate degradation pathways

L. Amino acid detailed degradation pathways.

Alanine (Ala)

Alanine is deaminated to pyruvate by direct oxidation via NAD-dependent alanine dehydrogenase. Pyruvate is then degraded as explained in Supp. Matt (section K).

Arginine (Arg)

Arginine is first deaminated to citrulline, which is decomposed into carbamoyl-P and L-ornithine (Fig. S2). Carbomoyl-P is a compound that releases bicarbonate, ammonium and ATP when decomposed enzymatically, providing the cell ATP in the hydrolytic step before redox reactions. L-ornithine is as well an AA but, as it only acts as an intermediate in Arginine degradation, we did not consider it as a starting AA in our network. L-ornithine has two degradation pathways. The first one consists in a deamination to L-proline, racemization to D-proline and then it follows proline usual degradation pathway (described later in this section). The other option yields D-alanine, acetyl-CoA and NADH (Uematsu, Sato, Hossain, Ikeda, & Hoshino, 2003).

Fig. S2. Arginine (Arg) degradation pathways considered in the metabolic network.

Aspartate (Asp)

Aspartate can be oxidatively deaminated with NAD+ to yield oxaloacetate, which is then decarboxylated to pyruvate. Aspartate can be as well desaturatively deaminated to fumarate, which is further reduced with NADH to succinate (Unden, Strecker, Kleefeld, & Kim, 2013). Succinate can be either an end product or further catabolised to yield propionate and CO_2 with ATP formation.

Cysteine (Cys)

Cysteine is converted into pyruvate and releases one molecule of hydrogen sulphide from Cysteine thiol group in carbon 3 (Loddeke et al., 2017). In this case one molecule of hydrogen sulphide is released as cysteine has a thiol group in carbon 3. Hydrogen sulphide is as weak acid that is considered to be excreted to the bulk without further transformation.

Glutamate (Glu)

Glutamate is mainly reported to be degraded in two ways (W. Buckel, 2001; Wolfgang Buckel & Barker, 1974). It might be converted to pyruvate and one acetate (not acetyl-CoA). Alternatively, Glu might be transformed to glutaconyl-CoA and then decarboxylated to crotonyl-CoA, which is then considered to be completely converted to butyrate. In this pathway, the decarboxylation of glutaconyl-CoA is reported to conserve energy in form of a proton translocation. Other reported degradation pathways yield 4-aminovalerate and 5-aminovalerate but, they are not included in our metabolic network as they are produced because they are produced as a reaction to an internal pH drop and against osmotic stress, respectively.

Glycine (Gly)

The most accepted degradation pathway for glycine is reduction and deamination to acetyl-P with NADH to yield acetate and ATP in a subsequent step (Andreesen, 1994). Other options include oxidation to CO_2 and ammonium (discarded as this pathway is reported when glycine is the only carbon source for microorganisms) (Andreesen, Bahl, & Gottschalk, 1989) and production of methylene-THF, CO_2 and ammonium (which occurs simultaneous to autotrophic pathways).

Histidine (His)

This AA is converted in several steps to yield glutamate and formamide (the amide of formic acid). Formamide is considered to be split into formate and ammonium without producing

energy (Kaminskas, Kimhi, & Magasanik, 1970; Prusiner & Milner, 1970; Sims, Sommers, & Konopka, 1986).

Lysine (Lys)

This AA has only one reported degradation pathway (Kreimeyer et al., 2007; Ramsay & Pullammanappallil, 2001). Lysine is oxidised with NAD+ to yield butyrate and acetate. One ATP molecule is yielded concomitantly.

Proline (Pro)

This AA has only one reported option of anaerobic degradation. It consists on the reduction of two molecules of proline to give two molecules of 5-aminovalerate, which react with themselves to finally yield acetate, propionate and n-valerate. The reaction is a dismutation reaction because one molecule acts as electron donor and the other as electron acceptor. One ATP is reported to be produced for each two molecules of 5-aminovalerate, giving a ratio of 0.5 ATP produced for each proline degraded (Barker, D'Ari, & Kahn, 1987).

Serine (Ser)

Serine is reported to have only one catabolic degradation possibility: deamination to yield pyruvate and ammonium (Sawers, 1998). Andreesen *et al.* (Andreesen et al., 1989) also reports its conversion to glycine and tetrahydrofuran (THF) but this option is related only with anabolic purposes and therefore not included.

Threonine (Thr)

This AA could potentially be degraded via five options of which only two were retained (Fig. S3) (Sawers, 1998). On the one hand, deamination to 2-oxobutyrate and then either amination to 2-aminobutyrate, which is excreted, or decarboxylation to propionyl-CoA and subsequent propionate and ATP production. In this last option, the enzyme complex in charge of the decarboxylation step is very similar to the pyruvate dehydrogenase complex and can even be the same enzyme acting on a different substrate. On the other hand, threonine might be oxidised with NAD^+ to 2-amino-3-ketobutyrate, which is afterwards split into acetyl-CoA and glycine. Alternatively, Thr is also reported to be directly split into acetaldehyde and glycine, but this option is not considered as acetaldehyde is not a common product of MCF and because it has a much lower energy yield compared to the other options available.

Fig. S3. Threonine (Thr) degradation pathways considered in the metabolic network.

Valine (Val), Isoleucine (Ile) and Leucine (Leu)

Due to their branched carbon skeleton, the products of these three AA (Fig. S4) are branched VFA (isobutyrate, isovalerate and isocaproate, respectively) (Elsden & Hilton, 1978). The pathways and the enzymatic mechanisms of degradation are also similar. All three AA can be oxidised but only one, Leucine, can be reduced.

Fig. S4. AA yielding branched VFA

They are first deaminated oxidatively (i.e. NADH is yielded, reaction 1 in Fig. S5) to a 2-oxoacid. In the oxidative branch (blue arrows in Fig. S5) the oxoacid is then decarboxylated with enzymes of the group 2-keto acid oxidoreductase (reaction 2 in Fig. S5). In this reaction, apart from losing one CO_2 molecule, they produce reduced ferredoxin and one CoA group is added to the carbon skeleton. The reaction scheme is the same as in pyruvate decarboxylation. In the last step cells conserve energy, as ATP is produced. As a result, the resulting VFA has one less carbon than the original AA.

However, as the net ATP production stoichiometry is one mole ATP for each mole AA degraded, the overall reaction is endergonic and none of the branched AA would be degraded into branched VFA. Thus, the oxidative branch can be divided in two steps: first an oxidative deamination and then a decarboxylation and ATP production altogether. The deamination part is significantly endergonic ($\Delta G'_m$=+25.6 kJ/mol for Valine and $\Delta G'_m$=+23.6 kJ/mol for isoleucine) while the decarboxylation is not exergonic enough to make the overall reaction exergonic ($\Delta G'_m$=-8.4 kJ/mol for isobutyrate production and $\Delta G'_m$=-14.2 kJ/mol for isovalerate production). All literature experiments on different proteins degradation report branched VFA as a product, indicating that, after all, branched AA degradation does occur in experiments (Breure, Beeftink, Verkuijlen, & Andel, 1986; Breure, Mooijman, & van Andel, 1986; Breure & van Andel, 1984; Breure, van Andel, Burger-Wiersma, Guijt, & Verkuijlen, 1985; Fang & Yu, 2002; Tan, Miyanaga, Uy, & Tanji, 2012; Yu & Fang, 2003). To reconcile these two in principle contradictory facts, we propose that part of the ATP generated in the second part of the branch is used to drive the endergonic deamination, in the fashion of the reverse electron transport (RET) mechanism (Elbehti, Brasseur, & Lemesle-Meunier, 2000; Stams & Plugge, 2009). A minimal net production of 0.25 ATP was selected to ensure that, even though internal concentrations vary, the global degradation reaction could be exergonic.

The reductive pathway starts after the reduction of the 2-oxo acid generated by deamination to form the corresponding 2-hydroxy acid (reaction 3 in Fig. S5). This compound is dehydrated, forming an enoate (reaction 4 in Fig. S5), which can be further reduced to yield a VFA with the same number of carbons as the original AA (reaction 5 in Fig. S5). However, the enoate reductase, requires a hydrogen atom in position 3, something that only Leucine can satisfy (Fig. S4) (Simon, Bader, Günther, Neumann, & Thanos, 1985).

Fig. S5. Branched-VFA producing AA degradation reaction scheme. Yellow arrows correspond to the oxidative pathway and green arrows to the reductive pathway.

Methionine (Met)

Methionine is initially transformed to 2-oxobutyrate and methanethiol (Met has a sulfur-containing functional group such as Cysteine but in this case is a thioester, not a thiol) (P. Bonnarme, Psoni, & Spinnler, 2000; Pascal Bonnarme, Lapadatescu, Yvon, & Spinnler, 2001). Methanethiol is considered to be excreted without further transformation. However,

it is not reported whether 2-oxobutyrate is excreted in this way or it is further transformed. We propose here that, in analogy with Val, Ile and Leu, 2-oxobutyrate is decarboxylated oxidatively in a reaction similar to pyruvate dehydrogenase, by the enzyme 2-oxobutanoate synthase. The products of this reaction are propionyl-CoA, CO_2 and Fd_{red}. Propionyl-CoA is proposed as well to yield ATP at the end of the pathway. 2-oxobutyrate could be instead reduced to crotonate, in a reaction scheme equal to leucine reduction to isocaproate (2-oxobutyrate has a hydrogen atom in position 3). Crotonate is then reduced to butyrate as in the butyrate yielding pathway from pyruvate. As in this last case, we consider that this highly exergonic step can lead via EB to H_2 production or to a proton translocation (section K).

Glutamine (Gln) and Asparagine (Asn)

These two AA are amides of Glutamate and Asparagate, respectively. They are deaminated in one step to their respective AA without the generation of reductive power.

3. ADDITIONAL INFORMATION OF THE SIMULATIONS.

M. Amino Acid profile of the simulated gelatine.

Simulations with the 9 different gelatine profiles of Fig. 3 were done at pH 7, and at the conditions of experiments A to F in Table 2, and compared with the experimental values. The root-square mean deviation (RMSD, Eq. S24) was used as a parameter to select the profile proving a best fit between the simulations and the experimental data.

$$RMSD = \sqrt{\frac{1}{n} \cdot \sum_{i=1}^{n} \left(\frac{\hat{y}_i - y_i}{y_i + y_{i,min}} \right)^2} \qquad \text{(S24)}$$

Where n is the number of data pairs, $\hat{y}_i$ is the model yield value, y_i is the experimental yield value and $y_{i,min}$ is the minimum experimental yield value of the different VFA. If there happens to be an experimental yield value of zero, the next value in increasing order would be chosen as minimum experimental value.

In Table S1 the RMSD values between the simulations with the different profiles and the experimental data are presented. Profile 5 provides the lowest average RMSD value for all the experimental data sets among the 9 different profiles.

Table S1. RMSD values between the different Breure experiments and the different AA profiles. The nomenclature of Table 2 is followed for naming the experiments.

	Experiment						
	A	**B**	**C**	**D**	**E**	**F**	**Average**
Profile 1	1.10	0.82	1.32	0.43	0.43	0.79	**0.81**
Profile 2	0.86	0.84	1.36	0.42	0.40	0.81	**0.78**
Profile 3	1.00	0.75	1.30	0.36	0.34	0.77	**0.75**
Profile 4	1.15	0.84	1.36	0.42	0.40	0.82	**0.83**
Profile 5	0.90	0.61	0.90	0.32	0.31	0.55	**0.60**
Profile 6	0.97	0.83	1.22	0.45	0.43	0.78	**0.78**
Profile 7	1.50	1.27	2.10	0.65	0.62	1.28	**1.24**
Profile 8	1.05	0.88	1.43	0.44	0.40	0.87	**0.85**
Profile 9	1.04	0.70	1.33	0.30	0.26	0.76	**0.73**

The comparison between the simulated yield values with AA profile 5 and the different experiment yields is shown in Fig. S6.

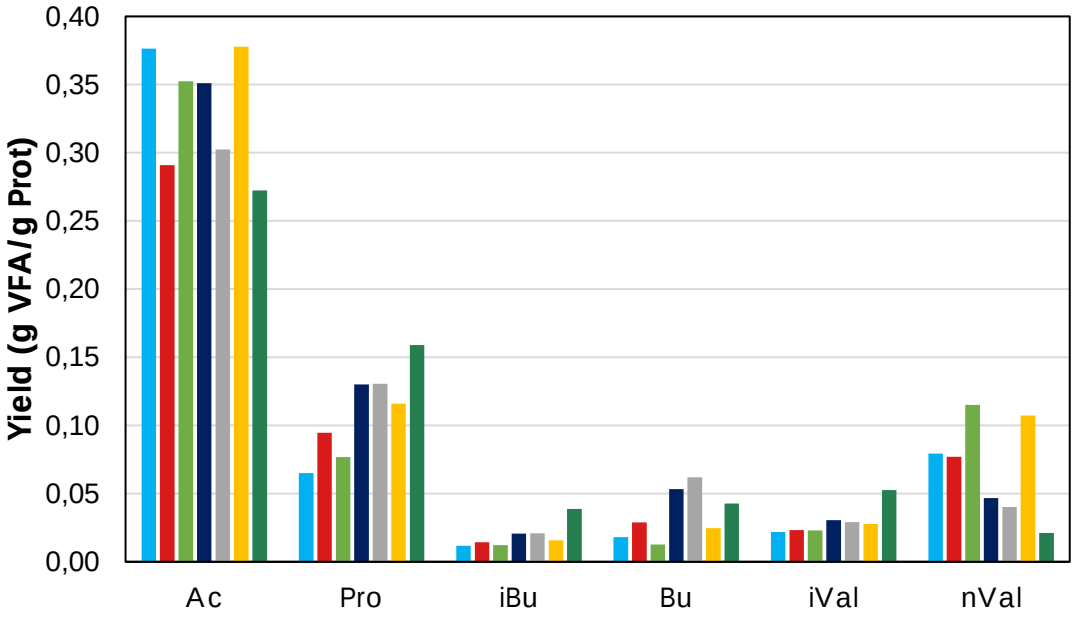

Fig. S6. Breure experimental results (Table 2 in the main text) at pH 7 and model results using Profile 5 gelatine (average value for the different experimental conditions of A-F). ■ A ■ B ■ C ■ D ■ E ■ F ■ Model results.

Profile 5 composition in AA, used in all the simulations, is shown in Table S2. Percentages are referred to molar basis.

Table S2. AA spectrum of gelatine profile 5 using in the simulations (molar basis) and molecular weight of a C-mol of that protein.

Arg	4.7%
Ala	2.7%
Asp	6.3%
Lys	3.3%
Glu	5.0%
Ser	5.3%
Thr	11.0%
Cys	8.0%
Gly	11.6%
Pro	5.6%
Val	6.0%
Ile	3.3%
Leu	4.0%
Met	3.0%

Gln	9.6%
Asn	6.3%
His	4.3%
MW (g/C-mol)	29.0

N. Mechanistic analysis the model outcome.

This section shows how mechanistic and exploitable information can be obtained from the proposed model. CSTR experiments at two pH values are simulated and we focus on analysing why the different AA are converted to their final products and how this stoichiometry is affected by pH. A simulation at a neutral value (pH 7) is first described, since most of the Breure experiments were done at this value, followed by a simulation at an acidic pH (value of 5.3) in order to compare with the low pH Breure experiments.

Neutral pH

Fig. S7 shows the product yields and also the origin of the different VFA (i.e. from which AA they are yielded). According to the model, glycine should not be consumed at all because its degradation reaction is endergonic.

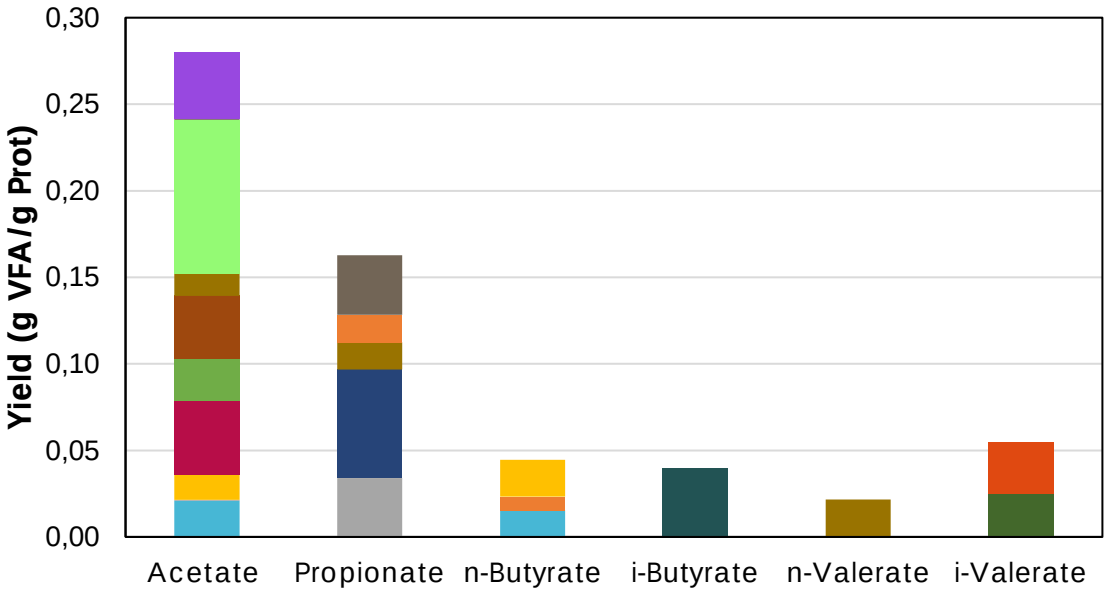

Fig. S7. Product yields for gelatine degradation in an CSTR at pH 7 predict by the model.

Arg Ala Asp Lys Glu Ser Thr Cys Gly Pro Val Ile Leu Met Gln Asn His

The information in Table S3 is very useful to explain the model solution. Asp is modelled to be degraded in a 98% to propionate (reaction 1 in Table S3) and just a 2% to acetate (reaction 2 in Table S3). Both reactions produce net ATP ($r_{ATP}>0$) but reaction 1 consumes NADH ($r_{NADH}<0$) while reaction 2 produces it ($r_{NADH}>0$). However, reaction 2 provides 39% less ATP than reaction 1. Why then is a fraction of Asp degraded to acetate? The reason is related with the opportunity cost in terms of ATP (i.e. ratio of the ATP rate difference and NADH rate difference or, alternatively, the ATP production rate lost for each unit of NADH production rate unit). Pro (reaction 3 in Table S3) consumes NADH, which indicates that to completely degrade Pro, other reactions should produce a sufficient NADH rate. This reaction has an ATP to consumed-NADH ratio of 0.26 mol ATP/mol NADH, a value higher than the opportunity cost of degrading aspartate to acetate instead of propionate. Therefore, it is globally worthwhile to sacrifice part of the possible ATP yielded by Asp as producing enough NADH to fully degrade Pro will produce extra ATP. For instance, if Asp rate increases to use the available NADH in Pro degradation and not to increase the propionate yield from Asp would represent a 4% increase in terms of extra ATP generated.

Table S3. Analysis of the steady station solution at pH7.

#		r_{NADH} ($mol_{NADH}/Lx \cdot h$)	r_{ATP} ($mol_{ATP}/Lx \cdot h$)	Z	r_{ATP}/r_{NADH} (mol_{ATP}/mol_{NADH})	Opportunity cost $\Delta r_{ATP}/\Delta r_{NADH}$ (mol_{ATP}/mol_{NADH})
1	Asp -> Prop	-0.154	0.178	0.976	1.15	
2	Asp -> Ac	0.154	0.109	0.024	0.71	0.22
3	Pro -> ½ Ac + ½ Prop + ½ n-Val	-0.069	0.018	1	0.26	
4	Ile -> i-Val	0.039	-0.006	1	-0.15	
5	Leu -> i-Val	0.048	-0.004	1	-0.09	

This is the case as well of Ile and Leu (reactions 4 and 5 in Table S3). Both AA produce NADH in their degradation but consume ATP. It seems counterintuitive at first sight to spend ATP degrading an AA when there is always the option of not consuming it. But the ATP to produced-NADH ratio is -0.09 and -0.15 for Leu and Ile, respectively, which is lower than the ATP to consumed-NADH ratio of Pro, meaning that it is profitable again to spend energy in degrading AA that produce NADH that will be consumed in the NADH-consuming degradation of Pro. For instance, if Ile was not consumed at all, only 44% of the Proline could be degraded and the ATP produced by these three AA would be an 54% lower.

Acidic pH

The different VFA yields are affected as follows when the pH changes from 7 to 5.3 (Fig. S8):

- Propionate, isobutyrate and isovalerate yields are basically the same in both cases.
- The yield of n-butyrate increases at pH 5 because there are AA that now yield it that before did not produce butyrate (Glu, Gln and His).
- The yield of n-valerate yield decreases because proline uptake rate is affected by the low pH value and is not fully consumed at pH 5 (Table S4).
- Acetate yield decreases both because part of AA that yield it are affected by the effect of a lower pH and because some AA changed their degradation option.

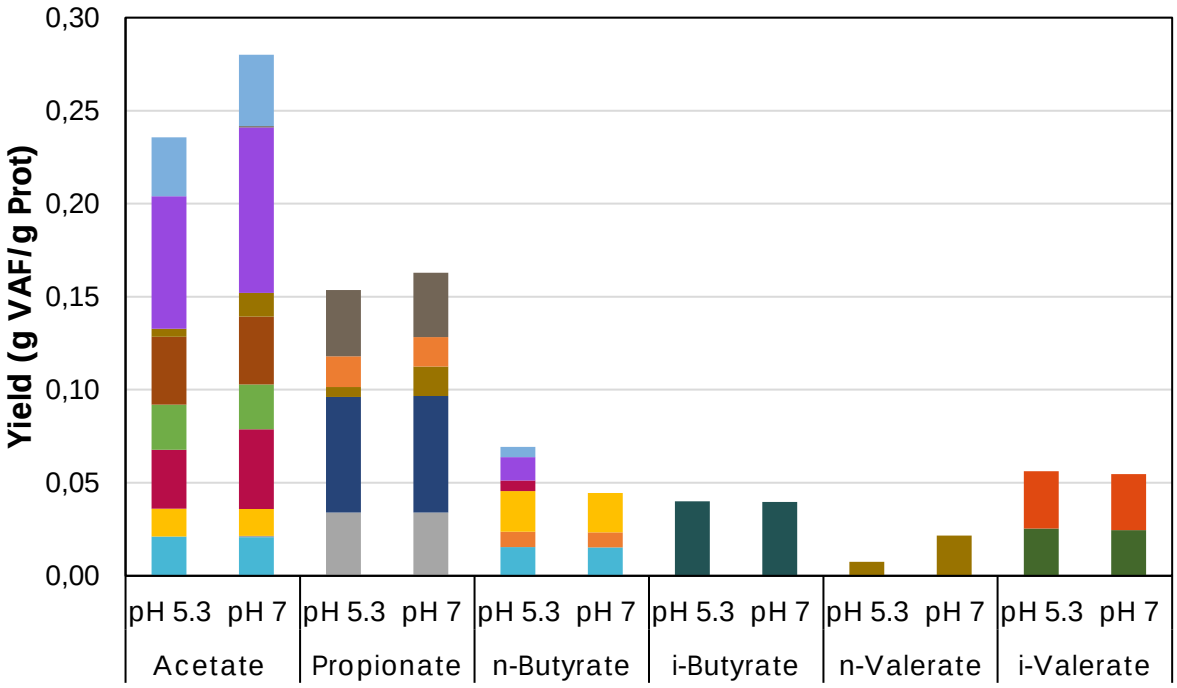

Fig. S8. Model results for gelatine degradation in an CSTR at pH 7 and pH 5.3. Product yields. Arg Ala Asp Lys Glu Ser Thr Cys Gly Pro Val Ile Leu Met Gln Asn His

At pH 5.3 there are two main products with similar yields (acetate and propionate) and the rest of VFA yields are at a certain distance and with similar values except for n-valerate. The results at a pH of 5.3 show that the biggest change in product spectrum with respect the simulation at pH 7 is the increase of 66% in the n-butyrate share and the 63% decrease of n-valerate product spectrum (Fig. S8). The acetate share is reduced as well but

only in a 11%. Regarding the conversion value the simulation at pH 5.3 indicates a degradation of 86.2%, a decrease of 8% compared to the simulation at pH 7.

Table S4. Relevant changes between pH 7 and pH 5.3 model results. Highlighted AA present different behaviour. P: produces NADH. C: consumes NADH.

AA	pH 7	NADH balance	Conversion	pH 5.3	NADH balance	Conversion
Asp	0.98 Prop + 0.02 Ac	C	97.7%	Prop	P	90.7%
Glu	2 Ac	-	95.5%	1.61 Ac + 0.19 n-But	C	81.6%
Pro	0.5 Ac + 0.5 Prop + 0.5 n-Val	P	98.9%	0.5 Ac + 0.5 Prop + 0.5 n-Val	P	32.3%
Gln	2 Ac (via Glut)	-	98.9%	1.61 Ac + 0.19 n-But (via Glu)	C	95.2%
Asn	0.98 Prop + 0.02 Ac (via Asp)	C	98.9%	Prop (via Asp)	P	94.8%
His	2 Ac (via Glut)	-	98.9%	1.61 Ac + 0.19 n-But (via Glu)	C	94.2%

A change in pH can modify the energetics of the different pathways and the AA uptake kinetics. For example, the energy associated with proton translocations (i.e. pmf) depends on pH and it is higher when the pH is more acidic (Eq. S15 and Fig. S9). In consequence, pathways associated with a proton translocation are favoured when pH drops. This is the case of the Glu conversion to n-butyrate, which has two proton translocations associated. At pH 7 it is completely degraded into acetate (no proton translocations associated) but at pH 5.3 part of it yields n-butyrate instead because now this pathway yields more ATP (Fig. S8 and Table S5). On the contrary, when pH rises those pathways are disfavoured as its energy production decreases. In the case of the Glu, changing the pH from 7 to 9 does not have an effect in its degradation because the pathway without proton translocations was already the preferred at pH 7.

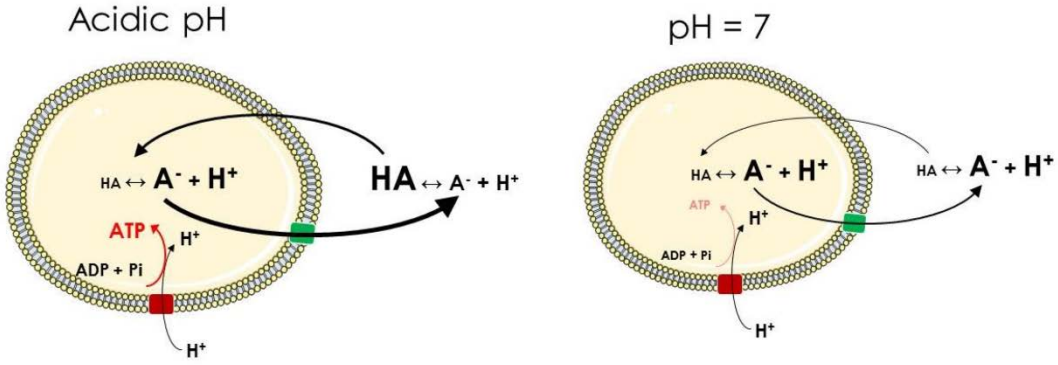

Fig. S9. Effect of an acidic pH on transport rates and pmf.

Changing the extracellular pH value also modifies the degree of dissociation of VFA (from 99.4% at pH 7 to 77.4% at pH 5.3 for acetate). As the protonated form of acids can freely diffuse towards the cytoplasm of cells, a decrease in pH will increase the diffusion-related transport rate of VFA inwards cells. In consequence cells will be forced to increase the energy-dependent active transport rate to avoid VFA accumulation in the cytoplasm (Fig. S9). The differences between the degrees of dissociation of the different VFA from pH 7 and a higher value is insignificant (from 99.4% at pH 7 to 100% at pH 9 for acetate). This implicates that changing the pH from 7 to an alkaline value has a very limited impact on transport energy expenditure and therefore also explains why there are no differences in the predicted yields between pH 7 ant higher pH values.

The relation between the energetics and the changes observed in the predicted yields can be understood analysing the model solution at steady state (Table S5). At pH 7 Glu was completely transformed into acetate (reaction 2 in Table S5) in an NADH-neutral reaction as it was the option with the highest ATP production rate associated. However, at pH 5.3 its NADH-consuming degradation into n-butyrate (reaction 1 in Table S4) is related with a higher ATP production rate (0.347 against 0.215 mol ATP/Lx h). Why is only 18% of Glu transformed to n-butyrate? Pro degradation also consumes NADH (reaction 3 in Table S5) and is in a competitive equilibrium with Glu: the opportunity cost of degrading Glu through reaction 2 instead of reaction 1 has the same value as the ATP generated per NADH consumed by Pro (Table S5). As a result, Pro is only degraded to a certain extent ($z<1$) because the global ATP production rate would be less if all the NADH was invested in degrading Pro and not into partially degrading Glu into n-butyrate.

Table S5. Analysis of the steady state solution for pH 5.3.

#		z	r_{NADH}	r_{ATP}	r_{ATP}/r_{NADH}	Opportunity cost
1	Glut -> n-but	0.19	-0.569	0.439	0.77	
2	Glut -> 2 Ac	0.87	0.000	0.267	-	0.30
3	Pro -> 0.5 Ac + 0.5 Pro + 0.5 Val	0.05	-1.236	0.377	0.30	
4	Asp -> Prop	1	-0.385	0.474	1.23	
5	Asp -> Ac	0	0.385	0.225	0.59	0.32

Asp degradation is as well different at pH 5.3 but its effects are less noticeable, because at pH 7 only 2% was degraded to yield acetate (Table S4) and not propionate, as both degrading options were in competitive equilibrium with Pro. In this case, that equilibrium does not longer exist because the opportunity cost of not degrading Asp into propionate has increased by 43% to 0.32 mol ATP/mol NADH and is now higher than the ATP to consumed-NADH ratio of Pro, meaning that cells would lose ATP if they invested it in degrading Pro instead of using it to produce propionate from Pro (Table S5). This increase of opportunity cost is as well related with the energetics changes when pH is modified. In the propionate-producing pathway from Asp there is one proton translocation associated and its contribution to the total ATP production rate of the pathway has increased by 41% due to the pH decrease, indicating that at pH 5.3 producing propionate is considerably more attractive than at pH 7.

O. Experimental yields from literature

In Table S6 details of the experimental data used in the main text to validate the model are given. Values are referred to grams of protein hydrolysed to better compare them with the model results, as the hydrolysis step is omitted in the model.

Table S6. VFA yields and operational conditions of the experiments used for the model validation. The same notation of the experiments as in the main text is followed. A (Breure & van Andel, 1984), B-E (Breure, Mooijman, et al., 1986), F (Breure, Beeftink, et al., 1986).

			Protein concentration	VFA Yields (g VFA/g Prot)					
Experiment	pH	D (h-1)	(g/L)	C2	C3	i-C4	C4	i-C5	C5
A	5.3	0.14	7.5	0.093	0.150	0.016	0.040	0.026	0.035
	7	0.23	7.5	0.376	0.065	0.018	0.012	0.079	0.022
B	7	0.10	5	0.291	0.095	0.029	0.014	0.077	0.023
C	7	0.15	5	0.352	0.077	0.013	0.012	0.115	0.023
D	7	0.20	5	0.351	0.130	0.053	0.021	0.047	0.031
E	7	0.20	5	0.302	0.131	0.062	0.021	0.040	0.029

F	5.3	0.12	7	0.161	0.144	0.016	0.045	0.027	0.044
	7	0.12	7	0.378	0.116	0.025	0.016	0.107	0.028

P. Changes in product yields with pH

In Fig. S10 the effect of pH in the model and experimental results is compared. All VFA except propionate agree on their tendencies with the pH change. Propionate, however, presents a different behaviour in the experimental data: while in one of the data sets (A) its yield increases notably when the pH drops from 7 to 5.3, in the other data set (F) its value does not increase as much (see section O for the experimental yields data). Acetate behaves equally in the model results and in the experiments: its yield decreases when pH decreases. However, it does it in a significantly higher degree in the experimental data, which is in accordance with the significantly overpredicted acetate yields in Fig. 6 on the main text. This issue might be related, as indicated in the main text, with the effect of pH on AA transport.

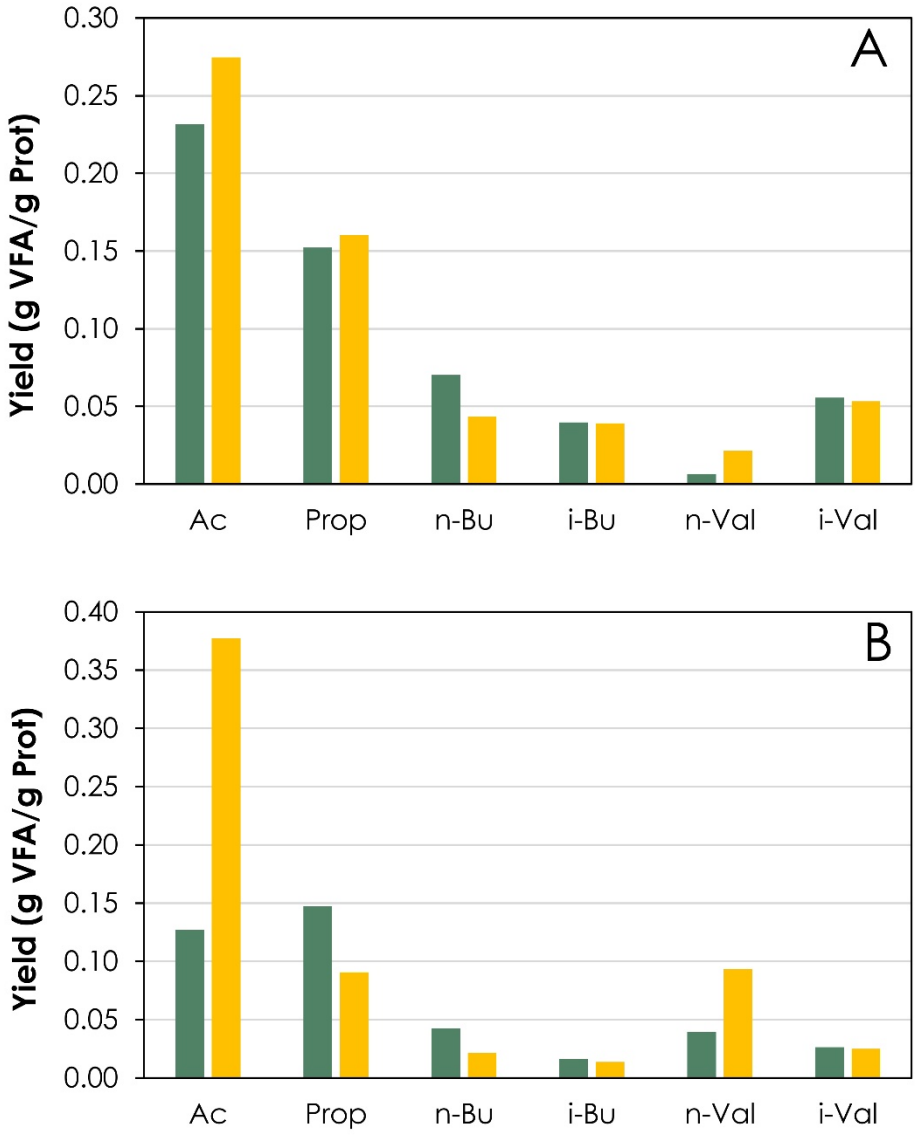

Fig. S10. Changes in product yields with pH. A: Model results. B: Average experimental results (A, F) (Breure, Beeftink, et al., 1986; Breure & van Andel, 1984). ■ pH 5.3 ■ pH 7.

Q. Comparison with previous works

The model selected different conversion stoichiometries for 7 AA when compared with the Ramsay and Pullammanappallil work (Ramsay & Pullammanappallil, 2001), representing 61.5% of all AA of the gelatine profile used in the simulations in molar basis

(Table S7). The objective of that work was not to explain mechanistically protein fermentation as it was focused on the anaerobic digestion to methane of proteins. The conversion stoichiometry of the different AA was selected based on literature information and it was considered to be fixed. They did not consider the NADH conservation as a constrain and the redox balance was closed by the production of H_2 from NADH and vice versa. However, it is accepted that H_2 cannot be yielded from NADH as it is clearly an endergonic reaction (see section H). Our model, on the contrary, does offer insight on the mechanisms of VFA production from AA and is able to predict how the conversion stoichiometry of the different AA changes with pH. These characteristics make it a more attractive as a design tool than the previous works available.

Table S7. Products of each AA and their role in the NADH balance. C: Consumes NADH. P: Produces NADH. N/C: not considered. Shaded cells correspond to AA where the end-products estimated by this work follow different pathways in comparison with Ramsay and Pullammanappallil (Ramsay & Pullammanappallil, 2001).

	Ramsay(Ramsay & Pullammanappallil, 2001)	NADH balance	Model	NADH balance
Arginine	0.5 Ac + 0.5 Prop + 0.5 n-Val	C	Ac + 0.5 n-But (via Ala)	P
Alanine	Ac	P	0.5 n-But	-
Aspartate	Ac	P	0.98 Prop + 0.02 Ac	C
Lysine	Ac + But	-	Ac + But	-
Glutamate	Ac + 0.5 n-But	C	2 Ac	-
Serine	Ac	-	Ac	-
Threonine	Ac + 0.5 n-But	C	Prop	-
Cysteine	Ac	-	Ac	-
Glycine	Ac	C	-	-
Proline	0.5 Ac + 0.5 Prop + 0.5 n-Val	C	0.5 Ac + 0.5 Prop + 0.5 n-Val	C
Valine	i-But	P	i-But	P
Isoleucine	i-Val	P	i-Val	P
Leucine	i-Val	P	i-Val	P

Methionine	Prop	-	Prop	-
Glutamine	N/C	-	2 Ac (via Glut)	-
Asparagine	N/C	-	Prop (via Asp)	C
Histidine	Ac + 0.5 n-But	-	2 Ac (via Glut)	-

R. Simulation results of gelatine with supplemented Thr.

Thr is an AA that is only predicted to yield propionate (Fig. S8). As the production of propionate from Thr is NADH-neutral (it does not produce or consume NADH, see section N), it is not expected to interfere with the degradation reactions of others AA. A simulation with doubled Thr concentration at pH 7 was run and the resulting yields are shown in Fig. S11. In this case the inlet substrate concentration is 7.7 g/L due to the increased Thr content. Propionate yield increased by 39% with respect to the standard gelatine degradation due to the increased content of Thr, which did not change its preferential degradation pathway (i.e. it is still fully degraded into propionate). The other VFA yields were not affected, as predicted, because Thr does not compete for NADH, the most explicit AA interaction. Asp and Asn are other AA yielding propionate (Fig. S8) but its degradation pathways are not NADH neutral. It is probable that their addition to gelatine would provoke changes in other VFA yields (e.g. less Pro consumption, as it also consumes NADH, with a concomitant n-valerate yield decrease), which makes the addition of Thr a more attractive option. This strategy could be used in the future when large amounts of isolated AA from waste-derived proteins are expected to be available (Tuck, Pérez, Horváth, Sheldon, & Poliakoff, 2012).

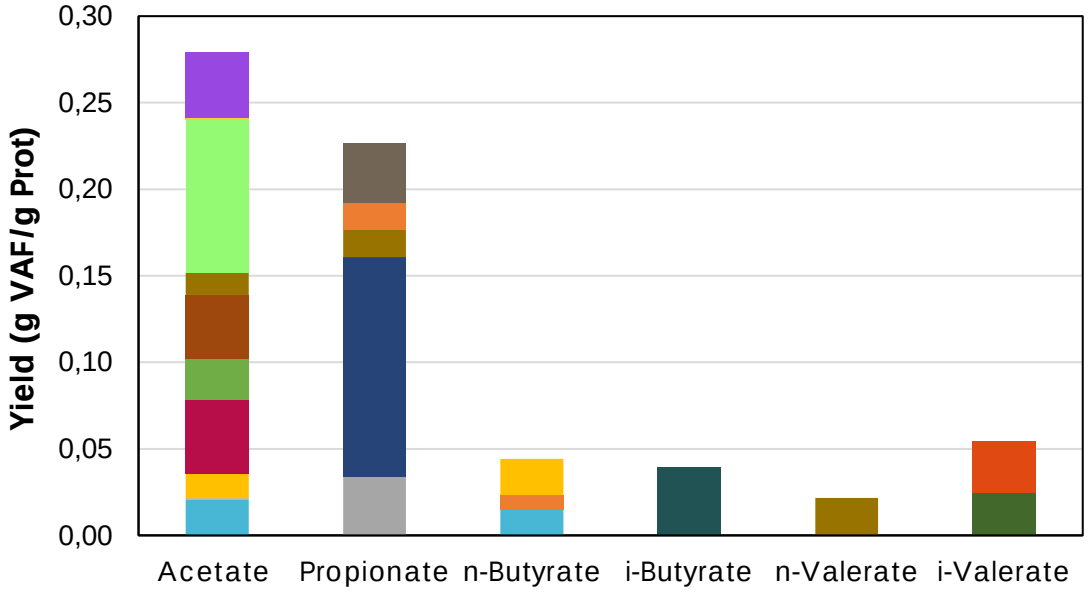

Fig. S11. Model results for gelatine degradation in an CSTR at pH 7 with supplemented Thr. Product yields. Arg Ala Asp Lys Glu Ser Thr Cys Gly Pro Val Ile Leu Met Gln Asn Hist

References

Andreesen, J. R. (1994). Glycine metabolism in anaerobes. *Antonie van Leeuwenhoek*, *66*(1–3), 223–237. https://doi.org/10.1007/BF00871641

Andreesen, J. R., Bahl, H., & Gottschalk, G. (1989). Introduction to the Physiology and Biochemistry of the Genus Clostridium. In N. P. M. and D. J. Clarke (Ed.), *Clostridia* (pp. 27–62). Springer Science + Business Media New York. https://doi.org/10.1007/978-1-4757-9718-3_2

Bar-Even, A., Flamholz, A., Noor, E., & Milo, R. (2012). Thermodynamic constraints shape the structure of carbon fixation pathways. *Biochimica et Biophysica Acta - Bioenergetics*, *1817*(9), 1646–1659. https://doi.org/10.1016/j.bbabio.2012.05.002

Barker, H. A., D'Ari, L., & Kahn, J. (1987). Enzymatic reactions in the degradation of 5-aminovalerate by Clostridium aminovalericum. *Journal of Biological Chemistry*, *262*(19), 8994–9003.

Berger, E. A. (1973). Different mechanisms of energy coupling for the active transport of proline and glutamine in Escherichia coli. *Proceedings of the National Academy of Sciences of the United States of America*, *70*(5), 1514–8. https://doi.org/10.1073/pnas.70.5.1514

Bonnarme, P., Lapadatescu, C., Yvon, M., & Spinnler, H. E. (2001). L-methionine degradation potentialities of cheese-ripening microorganisms. *Journal of Dairy Research*, *68*(4), 663–674. https://doi.org/10.1017/S002202990100509X

Bonnarme, P., Psoni, L., & Spinnler, H. E. (2000). Diversity of L-Methionine catabolism pathways in cheese-ripening bacteria. *Applied and Environmental Microbiology*, *66*(12), 5514–5517. https://doi.org/10.1128/AEM.66.12.5514-5517.2000

Breure, A. M., Beeftink, H. H., Verkuijlen, J., & Andel, J. G. Van. (1986). Acidogenic fermentation of protein / carbohydrate mixtures by bacterial populations adapted to one of the substrates in anaerobic chemostat cultures. *Applied Microbiology Biotechnology*, *23*, 245–249. https://doi.org/10.1007/BF00261923

Breure, A. M., Mooijman, K. A., & van Andel, J. G. (1986). Protein degradation in anaerobic digestion: influence of volatile fatty acids and carbohydrates on hydrolysis and acidogenic fermentation of gelatin. *Applied Microbiology and Biotechnology*, *24*, 426–431. https://doi.org/10.1007/BF00294602

Breure, A. M., & van Andel, J. G. (1984). Hydrolysis and acidogenic fermentation of a protein, gelatin, in an anaerobic continuous culture. *Applied Microbiology and Biotechnology*, *20*(1), 40–45. https://doi.org/10.1007/BF00254644

Breure, A. M., van Andel, J. G., Burger-Wiersma, T., Guijt, J., & Verkuijlen, J. (1985). Hydrolysis and acidogenic fermentation of gelatin under anaerobic conditions in a laboratory scale upflow reactor. *Applied Microbiology and Biotechnology*, *21*(1–2), 50–54. https://doi.org/10.1007/BF00252361

Buckel, W. (2001). Unusual enzymes involved in five pathways of glutamate fermentation. *Applied Microbiology and Biotechnology*, *57*(3), 263–273. https://doi.org/10.1007/s002530100773

Buckel, W., & Barker, H. A. (1974). Two Pathways of Glutamate Fermentation by Anaerobic Bacteria. *Journal of Bacteriology*, *117*(3), 1248–1260.

Buckel, W., & Thauer, R. K. (2013). Energy conservation via electron bifurcating ferredoxin reduction and proton/Na+ translocating ferredoxin oxidation. *Biochimica et Biophysica Acta (BBA) - Bioenergetics*, *1827*(2), 94–113. https://doi.org/http://dx.doi.org/10.1016/j.bbabio.2012.07.002

Buckel, W., & Thauer, R. K. (2018). Flavin-based electron bifurcation, ferredoxin, flavodoxin, and anaerobic respiration with protons (Ech) or NAD+(Rnf) as electron acceptors: A historical review. *Frontiers in Microbiology*, *9*(MAR). https://doi.org/10.3389/fmicb.2018.00401

Elbehti, A., Brasseur, G., & Lemesle-Meunier, D. (2000). First evidence for existence of an uphill electron transfer through the bc1 and NADH-Q oxidoreductase complexes of the acidophilic obligate chemolithotrophic ferrous ion-oxidizing bacterium Thiobacillus ferrooxidans. *Journal of Bacteriology*, *182*(12), 3602–3606. https://doi.org/10.1128/JB.182.12.3602-3606.2000

Elsden, S. R., & Hilton, M. G. (1978). Volatile acid production from threonine, valine, leucine and isoleucine by clostridia. *Archives of Microbiology*, *117*(2), 165–172. https://doi.org/10.1007/BF00402304

Fang, H. H. P., & Yu, H. (2002). Mesophilic acidification of gelatinaceous wastewater. *Journal of Biotechnology*, *93*(2), 99–108. https://doi.org/10.1016/S0168-1656(01)00397-2

Gary, C., Frossard, J., & Chenevard, D. (1995). Heat of combustion, degree of reduction and carbon content: 3 interrelated methods of estimating the construction cost of plant tissues. *Agronomie*, *15*(1), 59–69. https://doi.org/10.1051/agro:19950107

Gommers, P. J. F., Vanschie, B. J., Vandijken, J. P., & Kuenen, J. G. (1988). Biochemical Limits to Microbial-Growth Yields - an Analysis of Mixed Substrate Utilization. *Biotechnol Bioeng*, *32*(1), 86–94.

González-Cabaleiro, R., Lema, J. M., & Rodríguez, J. (2015). Metabolic Energy-Based Modelling Explains Product Yielding in Anaerobic Mixed Culture Fermentations. *PLoS ONE*, *10*(5), e0126739. https://doi.org/10.1371/journal.pone.0126739

González-Cabaleiro, R., Lema, J. M., Rodríguez, J., & Kleerebezem, R. (2013). Linking thermodynamics and kinetics to assess pathway reversibility in anaerobic bioprocesses. *Energy and Environmental Science*, *6*(12), 3780–3789. https://doi.org/10.1039/c3ee42754d

Guidotti, G. G., Borghetti, A. F., & Gazzola, G. C. (1978). The Regulation Of Amino Acid Transport in Animal Cells. *Biochimica et Biophysica*, *515*, 329–366.

Herrmann, G., Jayamani, E., Mai, G., & Buckel, W. (2008). Energy conservation via electron-transferring flavoprotein in anaerobic bacteria. *J Bacteriol*, *190*(3), 784–791. https://doi.org/10.1128/jb.01422-07

Heyne, R. I., de Vrij, W., Crielaard, W., & Konings, W. N. (1991). Sodium ion-dependent amino acid transport in membrane vesicles of Bacillus stearothermophilus. *Journal of Bacteriology*, *173*(2), 791–800. Retrieved from http://www.pubmedcentral.nih.gov/articlerender.fcgi?artid=207073&tool=pmcentrez&rendertype=abstract

Hoelzle, R. D., Virdis, B., & Batstone, D. J. (2014). Regulation Mechanisms in Mixed and Pure Culture Microbial Fermentation. *Biotechnology and Bioengineering*, *111*(11), 2139–2154. https://doi.org/10.1002/bit.25321

Kaminskas, E., Kimhi, Y., & Magasanik, B. (1970). Urocanase and N-formimino-L-

glutamate formiminohydrolase of Bacillus subtilis, two enzymes of the histidine degradation pathway. *Journal of Biological Chemistry*, *245*(14), 3536–3544.

Kleerebezem, R., Rodriguez, J., Temudo, M. F., & van Loosdrecht, M. C. (2008). Modeling mixed culture fermentations; the role of different electron carriers. *Water Sci Technol*, *57*(4), 493–497. https://doi.org/10.2166/wst.2008.094

Kreimeyer, A., Perret, A., Lechaplais, C., Vallenet, D., Médigue, C., Salanoubat, M., & Weissenbach, J. (2007). Identification of the last unknown genes in the fermentation pathway of lysine. *Journal of Biological Chemistry*, *282*(10), 7191–7197. https://doi.org/10.1074/jbc.M609829200

LaRowe, D. E., Dale, A. W., Amend, J. P., & Van Cappellen, P. (2012). Thermodynamic limitations on microbially catalyzed reaction rates. *Geochimica et Cosmochimica Acta*, *90*, 96–109. https://doi.org/10.1016/j.gca.2012.05.011

Li, F., Hinderberger, J., Seedorf, H., Zhang, J., Buckel, W., & Thauer, R. K. (2008). Coupled ferredoxin and crotonyl coenzyme A (CoA) reduction with NADH catalyzed by the butyryl-CoA dehydrogenase/Etf complex from Clostridium kluyveri. *J Bacteriol*, *190*(3), 843–850. https://doi.org/10.1128/jb.01417-07

Loddeke, M., Schneider, B., Oguri, T., Mehta, I., Xuan, Z., & Reitzer, L. (2017). Anaerobic Cysteine Degradation and Potential Metabolic Coordination in Salmonella enterica and Escherichia coli. *Journal of Bacteriology*, *199*(16), 1–16.

Meister, A. (2016). On the Enzymology of Amino Acid Transport Published by : American Association for the Advancement of Science Stable URL : http://www.jstor.org/stable/1735289 Linked references are available on JSTOR for this article : - On tlle Enzymology of Amino Acid Tr, *180*(4081), 33–39.

Oxender, D. L., & Christensen, H. N. (1963). Distinct Mediating Amino Systems for the Transport Acids by the Ehrlich Cell * of Neutral, *238*(11).

Padan, E., Zilberstein, D., & Schuldiner, S. (1981). pH homesstasis in bacteria. *BBA - Reviews on Biomembranes*, *650*(2–3), 151–166. https://doi.org/10.1016/0304-4157(81)90004-6

Peters, J. W., Miller, A. F., Jones, A. K., King, P. W., & Adams, M. W. W. (2016). Electron bifurcation. *Current Opinion in Chemical Biology*, *31*, 146–152. https://doi.org/10.1016/j.cbpa.2016.03.007

Poole, R. J. (1978). Energy Coupling for Membrane Transport. *Annual Review of Plant Physiology*, *29*(1), 437–460. https://doi.org/10.1146/annurev.pp.29.060178.002253

Prusiner, S., & Milner, L. (1970). A rapid radioactive assay for glutamine synthetase, glutaminase, asparagine synthetase, and asparaginase. *Analytical Biochemistry*, *37*(2), 429–438. https://doi.org/10.1016/0003-2697(70)90069-2

Ramsay, I. R., & Pullammanappallil, P. C. (2001). Protein degradation during anaerobic wastewater treatment: Derivation of stoichiometry. *Biodegradation*, *12*(4), 247–257. https://doi.org/10.1023/A:1013116728817

Regueira, A., González-Cabaleiro, R., Ofiţeru, I. D., Rodríguez, J., & Lema, J. M. (2018). Electron bifurcation mechanism and homoacetogenesis explain products yields in mixed culture anaerobic fermentations. *Water Research*, *141*, 5–13. https://doi.org/10.1016/j.watres.2018.05.013

Rodriguez, J., Kleerebezem, R., Lema, J. M., & van Loosdrecht, M. C. (2006). Modeling

product formation in anaerobic mixed culture fermentations. *Biotechnol Bioeng*, *93*(3), 592–606. https://doi.org/10.1002/bit.20765

Sawers, G. (1998). The anaerobic degradation of L-serine and L-threonine in enterobacteria: Networks of pathways and regulatory signals. *Archives of Microbiology*, *171*(1), 1–5. https://doi.org/10.1007/s002030050670

Simon, H., Bader, J., Günther, H., Neumann, S., & Thanos, J. (1985). Chirale Verbindungen durch biokatalytische Reduktionen. *Angewandte Chemie*, *97*(7), 541–555. https://doi.org/10.1002/ange.19850970705

Sims, G. K., Sommers, L. E., & Konopka, A. (1986). Degradation of pyridine by Micrococcus luteus isolated from soil. *Applied and Environmental Microbiology*, *51*(5), 963–968.

Stams, A. J. M., & Plugge, C. M. (2009). Electron transfer in syntrophic communities of anaerobic bacteria and archaea. *Nature Reviews Microbiology*, *7*(8), 568–577. https://doi.org/10.1038/nrmicro2166

Stouthamer, A. H. (1973). A theoretical study on the amount of ATP required for synthesis of microbial cell material. *Antonie van Leeuwenhoek*, *39*(1), 545–565. https://doi.org/10.1007/BF02578899

Tan, R., Miyanaga, K., Uy, D., & Tanji, Y. (2012). Effect of heat-alkaline treatment as a pretreatment method on volatile fatty acid production and protein degradation in excess sludge, pure proteins and pure cultures. *Bioresource Technology*, *118*, 390–398. https://doi.org/10.1016/j.biortech.2012.05.064

Temudo, M. F., Kleerebezem, R., & van Loosdrecht, M. (2007). Influence of the pH on (open) mixed culture fermentation of glucose: A chemostat study. *Biotechnology and Bioengineering*, *98*(1), 69–79. https://doi.org/10.1002/bit.21412

Tobajas, M., & Garcia-Calvo, E. (1999). Determination of biomass yield for growth of Candida utilis on glucose: Black box and metabolic descriptions. *World Journal of Microbiology and Biotechnology*, *15*(4), 431–438. https://doi.org/10.1023/A:1008911630776

Tuck, C. O., Pérez, E., Horváth, I. T., Sheldon, R. A., & Poliakoff, M. (2012). Valorization of Biomass : Deriving More Value from Waste. *Science*, *337*(November), 695–699.

Uematsu, H., Sato, N., Hossain, M. Z., Ikeda, T., & Hoshino, E. (2003). Degradation of arginine and other amino acids by butyrate-producing asaccharolytic anaerobic Gram-positive rods in periodontal pockets. *Archives of Oral Biology*, *48*(6), 423–429. https://doi.org/10.1016/S0003-9969(03)00031-1

Unden, G., Strecker, A., Kleefeld, A., & Kim, O. Bin. (2013). C4-Dicarboxylate Utilization in Aerobic and Anaerobic Growth. *EcoSal Plus*. https://doi.org/10.1128/ecosalplus.3.4.5

White, D., Drummond, J., & Fuqua, C. (2012). *The physiology and biochemistry of prokaryotes*. (D. White, Ed.) (4th ed.). New York: Oxford University Press. https://doi.org/10.1016/0306-3623(96)90070-1

Yu, H. Q., & Fang, H. H. P. (2003). Acidogenesis of gelatin-rich wastewater in an upflow anaerobic reactor: influence of pH and temperature. *Water Research*, *37*(1), 55–66. https://doi.org/http://dx.doi.org/10.1016/S0043-1354(02)00256-7

Zhang, F., Zhang, Y., Chen, M., van Loosdrecht, M. C., & Zeng, R. J. (2013). A modified metabolic model for mixed culture fermentation with energy conserving electron bifurcation reaction and metabolite transport energy. *Biotechnol Bioeng*, *110*(7), 1884–1894. https://doi.org/10.1002/bit.24855